MORPHOLOGICAL CHARACTERIZATION AND ANALYTICAL APPLICATION OF POLY(3,4-ETHYLENEDIOXYTHIOPHENE)-PRUSSIAN BLUE COMPOSITE FILMS ELECTRODEPOSITED IN SITU ON PLATINUM ELECTRODE CHIPS

Stelian Lupu[a, *], Boris Lakard[b], Jean-Yves Hihn[b], Jérôme Dejeu[c], Patrick Rougeot[c], Séverine Lallemand[b]

[a] *Department of Analytical Chemistry and Instrumental Analysis, Faculty of Applied Chemistry and Materials Science, University Politehnica of Bucharest, Polizu Street 1-5, 011061 Bucharest, Romania*

[b] *Institut UTINAM, CNRS-UMR 6213, Université de Franche-Comté, 16 route de Gray, Besançon Cedex 25030, France*

[c] *Institut FEMTO-ST, CNRS-UFC-ENSMM-UTBM, AS2M Department, 24 rue Alain Savary, 25000 Besançon, France.*

Abstract

Electrochemical in situ preparation and morphological characterization of inorganic redox material-organic conducting polymer coatings as thin films on platinum electrodes are presented. Composite inorganic-organic coatings consist of Prussian blue (PB) and [poly(3,4-ethylenedioxythiophene)] (PEDOT), and PEDOT organic polymers doped with ferricyanide (PEDOT-FeCN). The PEDOT coating deposited from an aqueous solution containing the EDOT monomer and $LiClO_4$ as supporting electrolyte was used as a "reference" material (PEDOT-ClO_4). The composite coatings were prepared by electrochemical methods on platinum electrode chips, which consist of a 150 nm Pt layer deposited on 100-oriented standard 3'' silicon wafers. Electrochemical behavior of the composite inorganic-organic coatings is based mainly on inorganic component redox reactions. Different surface properties of the composite materials were studied. Thus, the roughness of the deposited films was measured by both atomic force microscopy (AFM) and profilometry, leading to roughness values ranging from 3 nm to

* Corresponding author. Phone: +40 21 4023886; fax: +40 21 3111796 , *E-mail address*: stelianl@yahoo.com

217 nm for PEDOT-ClO_4, and PEDOT-FeCN and PEDOT-PB coatings, respectively. AFM and Scanning Electron Microscopy pictures were also produced to characterize the film morphologies, and revealed a granular pattern of the deposited inorganic component inside the organic polymer matrix. Moreover, the adhesion properties of the composites were studied by AFM and proved to be very different from one material to the other depending on the film structure. The electrochemical responses of these composite coatings to H_2O_2 reduction were also investigated using chronoamperometry. A linear response over a concentration range from 1 10^{-4} to 1 10^{-5} M and a detection limit of 10 μM were obtained.

Keywords: photolithography, atomic force microscopy, poly(3,4-ethylenedioxythiophene), Prussian Blue, composite thin films

1. Introduction

Polymer-based nanocomposites have become a prominent area of research and development in the field of nanotechnologies due to their chemical and physical properties that can be tailored for particular needs. Various materials like metals (gold, platinum), carbon, and organic conducting polymers have been used to prepare nanocomposite materials such as nanoparticles [1], nanotubes [2], molecularly imprinted polymers [3], and multilayers [4]. These composites based on organic polymers are promising for a variety of applications including optical and electronic devices, micromanipulation, chemical and biomedical analysis.

Conducting polymers have been used in sensor technology thanks to their optical and electronic properties [5-9]. Research carried out recently in electrochemical sensor technology revealed that modification of the electrode surfaces with organic-inorganic coatings avoids the drawbacks associated with bare electrodes. For instance, inorganic coatings consisting of transition metal hexacyanoferrates have been used in preparation of various sensors and biosensors based on electrochemical and optical transducers [10-19]. One of the inorganic modifiers, Prussian blue (PB, ferric ferrocyanide $Fe_4^{III}[Fe^{II}(CN)_6]_3$) is a mixed-valence compound that can be deposited on the electrode surface as an electroactive film. The chemical formulations of PB, referred to as “water insoluble PB”, $Fe_4^{III}[Fe^{II}(CN)_6]_3$ i.e. without potassium, and “water soluble

PB", $KFe^{III}[Fe^{II}(CN)_6]$, respectively, were used to describe the formation of PB [20]. The soluble form of PB was supposed to form in the presence of a potassium ion excess. A colorless compound called Prussian White (PW) is obtained by reduction of PB, while oxidation of PB yields Berlin Green (BG). PB deposited as thin films onto Pt electrodes typically displays two redox waves at ca. 0.2 V and 0.85 V vs. SCE, respectively. These waves correspond to the reduction of PB to PW and to the oxidation of PB to BG, respectively. These redox processes can be described for the soluble form of PB according to the following reactions [20, 21]:

• redox wave corresponding to the PB/PW system at ca. 0.2 V vs. SCE:

$$KFe^{III}[Fe^{II}(CN)_6] + e^- + K^+ \quad \Leftrightarrow \quad K_2Fe^{II}[Fe^{II}(CN)_6] \qquad (1)$$

• redox wave corresponding to the PB/BG system at ca. 0.85 V vs. SCE:

$$KFe^{III}[Fe^{II}(CN)_6] - e^- - K^+ \quad \Leftrightarrow \quad Fe^{III}[Fe^{III}(CN)_6] \qquad (2)$$

Composite materials based on transition metal hexacyanoferrates and conducting polymers have been recently prepared in various configurations on electrode surfaces [22-34]. The inorganic redox mediator maintained its electrocatalytic activity upon immobilization, and the organic component increased the stability of the coating in both organic media and aqueous solutions. The presence of both components in these materials allowed the preparation of stable, highly conducting, and selective coatings on electrode surfaces.

The main aim of this paper is to provide a full morphological characterization of composite materials consisting of PB and poly(3,4-ethylenedioxythiophene) (PEDOT) deposited as thin films on platinum electrode chips. The choice of inorganic and organic components for preparation of these composite materials is based on the excellent stability of the PEDOT layer in aqueous solution and its doped state [35-37], and the electrocatalytic activity of PB [38, 39], respectively. The PEDOT organic component is in its conducting state in the potential region where the PB inorganic component exhibits its good electrocatalytic activity. Therefore a synergistic effect could be expected, and the composite material should exhibit electrochemical properties and surface adhesion features. The approach used for preparation of these composite coatings enables surface characterization of each intermediate composite material.

To this end, Pt electrode chips were modified with PEDOT-only films as well as composite inorganic-organic PEDOT-FeCN and PEDOT-PB films. The electrochemical properties of these modified electrodes have been investigated by cyclic voltammetry (CV) in acidic aqueous solutions. The surface properties of these films have been also investigated by non-contact 3D profilometry, atomic force microscopy (AFM), and scanning electron microscopy (SEM). Furthermore, the electrochemical properties of these composite materials, deposited on Pt electrode, for hydrogen peroxide reduction have been also investigated.

2. Experimental details

2.1. Materials

All chemicals were used as received without any further purification. 3,4-ethylenedioxythiophene (EDOT, Aldrich) was used for electrochemical preparation of the corresponding polymer. Deionized water (Millipore) was always used to prepare aqueous solutions. The wafers used for fabrication of the working electrodes were 1 0 0-oriented standard 3'' type silicon wafers (thickness: 380 µm, p type, dopant: B, resistivity: 0.015 Ω.cm, from the Institute of Electronic Materials Technology).

2.2. Electrochemical measurements

Electrochemical experiments were carried out with a Voltalab potentiostat/galvanostat PGZ301 (Radiometer, France) coupled to a PC running the VoltaMaster software. All electrochemical measurements were performed using a single-compartment cell with three electrodes, at room temperature. The electrodes used were: a platinum electrode chip as a working electrode, a saturated calomel electrode, SCE, as a reference electrode (Metrohm), and a platinum wire (Metrohm) as an auxiliary electrode. Before each electrochemical measurement, the surface of the working electrode chip was checked by cyclic voltammetry in aqueous solution containing 1 mM $K_3Fe(CN)_6$ and 0.1 M KCl. A 2-mm diameter Pt rotating disk electrode was also used as a working electrode for electrochemical detection of hydrogen peroxide by chronoamperometry. The surface of the rotating Pt electrode was polished with alumina powder to a mirror finish prior to the electrochemical measurements. Chronoamperometry was conducted at the Pt

rotating disk electrode, modified with the composite materials, by holding electrode potential at 0.00 V vs. Ag/AgCl during the experiment at a rotation speed of 2000 rpm. The solutions were bubbled with high purity nitrogen, and a nitrogen flow was maintained over the solution during the measurements.

2.3. Fabrication of platinum electrode chips

The working electrode used for deposition of the composite coatings was elaborated using microsystem technologies, and in particular a lift-off process that consists in photolithography followed by platinum sputtering on a SiO_2 wafer. This technique made it possible to fabricate a flat platinum electrode (Figure 1) which was very useful for characterization of composites using surface analysis methods such as AFM, SEM or profilometry. The first step of the fabrication process consisted in drawing the required pattern with a commercial mask design software Cadence. A Cr/Glass mask, on which the shape of the pattern was drawn, was then made with an electromask optical pattern generator. The process started with a 100-oriented standard 3" silicon wafer, thermally wet-oxidized, at 1200°C in water vapor, in order to produce a 1.3 µm thickness SiO_2 layer. Next, a 1.4 µm thickness layer of negative photoresist (AZ 5214, from Clariant), suitable for lift-off, was deposited by spin coating. After that, the wafer was exposed with the mask to a 36 mJ/cm^2 UV radiation flux delivered by an EVG 620 apparatus, and then, without any mask, to a 210 mJ/cm^2 UV radiation flux. Thus the pattern was transferred to the resist, which was then developed, using AZ 726 developer, to dissolve the resist where the metal was deposited. A magnetron sputtering (Alcatel SCM 441 apparatus) was then used to coat microsystems with titanium (30 nm, used to improve platinum layer), then platinum (150 nm). The fabrication parameters for Pt and Ti films were: base pressure: 4.6×10^{-7} mbar, pressure (Ar) during sputtering: 5×10^{-3} mbar, power: 150W, target material purity: 99.99%. The remaining resist layer was then dissolved using acetone. After these microsystems have been fabricated, the pattern and dimensions are controlled using an optical microscope. More details about the microsystem fabrication can be found in a previous paper [40].

Figure 1 near here

2.4. Surface analysis of the composite materials

The coatings were also examined with a commercial Atomic Force Microscope (stand-alone SMENA scanning probe microscope NT-MDT, Russian). The experiments were conducted under a controlled environment with a laminar flow (with 30 % and 25°C humidity). The morphology and force measurements performed on this AFM, which were taken on the "Nanorol platform", were based on the measurement of the AFM cantilever deformation with a laser deflection sensor.

For the force measurement, the silicon rectangular AFM cantilever, with a stiffness of 0.3 N/m, was fixed, and the substrate moved vertically. Measurements were performed with a cantilever where a borosilicate sphere (r = 5 µm radius) was glued on the free extremity and below it (Novascan Technologies, Ames, USA). Distance-force curves were created to measure the approach force (pull-in force) when the sphere approaches the sample, and the adhesion force (pull-off force) when the sphere leaves the surface during sample retraction. Ten measurements were taken at different points on the same sample with a driving speed of 0.2 µm/s. Sample topography was analyzed with a Budget Sensors cantilever (stiffness 0.2 N/m) in contact mode.

Polymer morphology examinations were also performed using a high-resolution scanning electron microscope. Once synthesized and dried, the coatings were examined in a LEO microscope (Scanning Electron Microscopy LEO stereoscan 440, manufactured by Zeiss–Leica, Köln, Germany) with an electron beam energy of 15 keV.

Thickness and roughness of the polymer films were determined both by atomic force microscopy and by a stylus-based mechanical probe profiler (Alpha-Step IQ, KLA Tencor).

The non-contact 3D profilometry study was performed with the Infinite Focus metrology system developed by Alicona (Austria). Infinite Focus is an optical 3D measurement device that acquires a dataset at a high depth of focus similar to the SEM. The measurement of wear volume is achieved with a topomicroscope Infinite focus ® Alicona (Austria).

2.5. Deposition procedure of PEDOT-PB composite films

The PEDOT-PB composite inorganic-organic coatings were prepared by a two-step method, previously used for modification of conventional-size Pt electrodes and Au disk microelectrode arrays [34, 41, 42]. In this work, the concentration of Fe^{3+} ions and the number of deposition potential scans were changed. This procedure was then applied to Pt electrode chips in order to prepare the composite coatings for surface analysis. For these reasons the experimental details of the preparation procedures are presented hereafter. Firstly, the PEDOT layer was electrodeposited from an aqueous solution containing 0.01 M EDOT and 0.1 M $K_3[Fe(CN)_6]$ as a supporting electrolyte by potential cycling in the potential range from open circuit potential, OCP, to +1.0 V and reversed back to -0.6 V, at a scan rate of 0.05 V s^{-1} for 5 or 10 consecutive scans, respectively. The modified electrode obtained in the first step is referred to as Pt/PEDOT-FeCN. In the second step, the Pt/PEDOT-FeCN modified electrode was immersed in 0.002 M $FeCl_3$, 0.1 M KCl and 0.01 M HCl aqueous solution, and the electrode potential was scanned from 0.6 to -0.2 V at a scan rate of 0.05 V s^{-1} for 5 or 10 consecutive scans, respectively. The soluble PB is formed inside the PEDOT matrix during this last potential cycling. The resulting modified electrode is referred to as Pt/PEDOT-PB. The PEDOT-only coating was prepared by electrochemical polymerization of the EDOT monomer in a solution containing 0.01 M EDOT and 0.1 M $LiClO_4$ as a supporting electrolyte by potential cycling in the potential range from -0.6 to +1.0 V, for 5 or 10 consecutive scans, respectively. This modified electrode is referred to as Pt/PEDOT-ClO_4, and was considered as a reference material in this study.

3. Results and Discussion

3.1. Electrochemical preparation and characterization of PEDOT-PB composite coating modified electrode chips

Fig. 2 shows the CV recorded during electrochemical deposition of PEDOT-only coating performed on Pt electrode chips using 5 (see Fig. 2A) and 10 (see Fig. 2B) consecutive scans, respectively. Polymerization of EDOT takes place in the potential range from 0.85 to 1.00 V, as can be seen from the increase in anodic current.

Figure 2 near here

The resulting PEDOT-ClO_4 coating was considered as a reference material in this present study, and was further investigated using non-contact 3D profilometry, AFM, and SEM, as described in the next section.

The PEDOT-FeCN composite coating was prepared by electrochemical polymerization of the corresponding monomer in the presence of 0.1 M $K_3Fe(CN)_6$. Fig. 3 reports the cyclic voltammograms recorded during electrochemical polymerisation. The presence of the inorganic redox anion results in a peak-shaped voltammogram. Electrochemical polymerization of EDOT occurs in the potential range 0.85 – 1.0 V in the presence of ferricyanide ions, and thus the resulting organic polymer is doped with counterions from the electrolyte solution. In this case, oxidation of EDOT to PEDOT is mediated by ferricyanide ions. This result is supported by the presence of a large peak (see Fig. 3) that corresponds to oxidation of ferrocyanide ions formed during mediated oxidation of EDOT. It should be noted that the very first scan is started from OCP, which is ca. 0.4 V, towards the anodic limit of 1.0 V. Ferrocyanide ions are not present in the initial solution and are formed only in the oxidation of EDOT. Their reduction produces a cathodic peak located at ca. 0.1 V in the backward scan. Thus, the shape of the cyclic voltammograms in Figure 3 illustrates the difference in the two PEDOT growth mechanisms, i.e. PEDOT deposition in the presence of perchlorate ions and ferricyanide ions, respectively. These electrochemical features are supported by the morphological characterization results presented in Section 3.2. This modified electrode is referred to as Pt/PEDOT-FeCN. The experimental preparation procedure was applied for modification of the Pt electrode chips for 5 and 10 consecutive potential cycles, respectively.

Figure 3 near here

After deposition of PEDOT-FeCN coating, the modified electrode chips were immersed in Fe^{3+} containing solution to prepare the “soluble” PB layer. Fig. 4 reports the cyclic voltammograms recorded at the Pt/PEDOT-FeCN modified electrodes in aqueous solution containing 0.002 M $FeCl_3$, 0.1 M KCl and 0.01 M HCl.

Figure 4 near here

A redox wave consisting of a cathodic peak at 0.15 V and the corresponding anodic peak located at 0.18 V can be observed. The cathodic peak is ascribed to the reduction of PB to PW, while the corresponding anodic peak is ascribed to the oxidation of PW to PB, respectively. A peak potential difference of about 30 mV between these peaks was observed, which can attest to the presence of redox species attached to the electrode surface. However, this value is higher than that predicted by theory, i.e. 0 V, a difference that can imply some kinetic limitations in the redox reactions of PB/PW redox systems induced by the presence of the organic matrix hindering the free motion of potassium ions required according to equation (1). This redox wave is therefore ascribed to the PB/PW redox system. Both the cathodic and anodic peak currents increase during the potential cycling, attesting to the formation of PB inside the organic matrix. Thus, the in situ formation of the soluble form of PB is clearly demonstrated. These results demonstrate the possibility of controlling the thickness of the composite film by the number of potential scans.

The Pt/PEDOT-PB modified electrode chips were then characterized in aqueous solution containing 0.1 M KCl and 0.01 M HCl (see Fig. 5).

Figure 5 near here

A redox wave situated at 0.2 V for both modified electrodes can be observed in Fig. 5. This redox wave is ascribed to the PB/PW redox system. The values of the anodic and cathodic peak currents for each modified electrode are proportional to the potential cycle numbers used during the preparation procedures (see Figure 5C). This behavior was expected due to the different numbers of potential scans applied in the preparation of each modified electrode, i.e. 5 scans and 10 scans, respectively. The stability of this redox wave is excellent attesting that the electroactive species are irreversibly incorporated inside the organic polymer matrix, but maintaining their electroactivity under these experimental conditions. Electrode potential was scanned up to 1.0 V in order to check the second pair of voltammetric peaks with respect to the redox reaction of low spin iron ions, i.e. the PB/BG redox reaction. The second redox wave, which is

usually located at ca. 0.85 V for pure PB films and corresponds to the PB/BG redox system, cannot be observed in Figure 5, suggesting that this redox system is not electroactive under these experimental conditions.

3.2. Surface analysis of the inorganic-organic composite materials

3.2.a. Morphology of the composite films:

The AFM experiments were performed on the composite materials electrodeposited at different points in the sample (minimum 3 points). During the scan, the topographic map of the surface was obtained by the vertical displacement of the cantilever and thus of the scanner. For the same experiments, all the morphologies obtained by the AFM are similar, and only one of each is presented in Figure 6. SEM experiments were also conducted on the same samples to obtain additional information (Figure 7).

Figure 6 and Figure 7 near here

The AFM and SEM pictures showed a granular structure for each sample. The smallest grain size was obtained for PEDOT-$LiClO_4$. On the contrary, PEDOT-FeCN and PEDOT-PB films are very similar even if PEDOT-FeCN contains more aggregates in its structure. Consequently, these data revealed an important influence of the doping counter-anion salt. The differences in morphology can be explained by the size of the ions adsorbed during film electrodeposition since ClO_4^- ions are far smaller than the others ions. For PEDOT-FeCN and PEDOT-PB composite materials, the similar morphology is the consequence of their protocol of elaboration. Indeed, the PEDOT-BP films were obtained from the PEDOT-FeCN after an immersion in $FeCl_3$ containing solution.

Moreover, AFM and SEM pictures showed a rough relief, with a strong increase in heterogeneities with the thickness of the film. The difference in morphology between the different composite films also increases with the number of scans. Thus, after 10 scans, an increase of aggregation and height (of nearly twice) of the initial bumps (5 scans) was observed for PEDOT-PB and PEDOT-FeCN composites, whereas the height of the PEDOT/$LiClO_4$ films increased slightly but exhibit less aggregation.

3.2.b. Composite film roughness

The roughness of the platinum substrate and the different composite films were investigated using both a stylus-based mechanical probe profiler and an AFM (Table 1). Both average roughness (Ra) and peak to peak roughness (Rq) were estimated using the two methods, whereas sample height (H) was only estimated by non-contact 3D profilometry.

Table 1 near here

Table 1 shows that the roughness measured by AFM is always greater than the roughness measured by 3D profilometry. However, the same tendencies can be deduced from each type of measurement, and so the two methods can be considered as corroborating. Moreover, roughness of the PEDOT-ClO_4 composites is far less than roughness of PEDOT-FeCN and PEDOT-PB films, whatever the number of scans. Comparison between PEDOT-FeCN and PEDOT-PB composites shows that roughness is less for the latter. A decrease in thickness from PEDOT-FeCN to PEDOT-PB can be also observed from Table 1. This behavior is a consequence of the structuration at a nano-scale of the inorganic component PB within the PEDOT matrix during the second step of the preparation procedure. It may be possible that some excess ferricyanide ions are expelled off from the PEDOT-FeCN coating surface during the in situ preparation of PB inside the PEDOT matrix. This assertion is supported by the shape of the redox wave located at ca. 0.15 V in Figure 4, which becomes narrower with increasing scan numbers. Thus, both in situ formation and nanostructuration of PB inside the PEDOT matrix take place during the second step of the preparation procedure. Consequently, it can be deduced that incorporation of the inorganic mediator in the organic polymer decreases surface roughness, a fact that could be interesting when preparing smooth samples. It can also be observed that increasing the number of deposition scans from 5 to 10 results in an increase in both thickness and roughness for each type of composite.

3.2.c. Composite film adhesion properties

Approach and adhesion forces, referred to as pull-in forces and pull-off forces respectively, were measured for all polymer coatings versus and their salt electrolyte

and number of cycle depositions. The experimental curves are presented in Figure 8. Figure 8a indicates an influence of the number of cycles on the pull-in and pull-off force. Indeed, the pull-in and pull-off force increases from -62 to -2 nN and from -139 to -67 nN, respectively, when the number of cycles increases from 5 to 10 for PEDOT-ClO_4^- films. The electrolyte salt (Figure 8b) also influences the force between a borosilicate sphere and the sample. The average value of the different measurements at different electrodeposition scan numbers and salt conditions are summarized in Table 2. From this table, it can also be noted that the adhesion force measured between the cantilever and the PEDOT composites was very inferior to that measured between the free polymer substrate and the cantilever (near five times less). Consequently, when applied to micromanipulation, the PEDOT film electrodeposited on the gripper end-effectors could prove interesting for decreasing drastically the adhesion force.

Figure 8 near here
Table 2 near here

Moreover, pull-off decrease can be explained by an increase in roughness of the PEDOT-PB and PEDOT-ClO_4 films. More precisely, this pull-off decrease is probably due to modification of the surface (increase in number of bumps and bump height). For the PEDOT-FeCN (10 scans), bump coalescence and surface leveling have been observed in the AFM and SEM pictures (Figures 6b, 6b' and 7b), with the exception of the presence of a few holes. Consequently, when force-distance measurements are taken, the latter sample is near a surface with fewer structures and thus adhesion force is higher.

For pull-in variations, internal ion composition in the sample accounts for the measured difference. Indeed, for PEDOT-FeCN samples, the ions are in the film, so ions are hard to attain, thus resulting in a small pull-in force. On the contrary, the PB grains are developed on the film and can interact with the AFM cantilever. For the PEDOT-ClO_4 composite, film thickness is smaller thus allowing the ion to create interactions with the cantilever.

3.3. Electrochemical detection of hydrogen peroxide at Pt/PEDOT-PB modified electrodes

The electrochemical properties of the composite coatings were further investigated with respect to possible analytical applications. To this purpose, electrochemical determination of H_2O_2 at a rotating Pt (2-mm disk)/PEDOT-PB composite modified electrode was carried out in aqueous potassium phosphate buffer solution (pH = 7.2) using chronoamperometry at a working potential value of 0.00 V vs. Ag/AgCl. Fig. 9A shows the chronoamperogram for electrochemical reduction of H_2O_2 at PEDOT-PB composite coating prepared according to the preparation procedure described in the Experimental section. The modified electrode presented a current response after addition of H_2O_2 by an increment of 10 μM. After four additions (10 μM each), the electrode response is less well defined. A plot of the current vs. concentration (see the inset in Fig. 9A) was found to be linear in the 10 to 50 μM range with correlation coefficient (R^2) 0.9878. Sensitivity, determined from the slope of the calibration plot divided by the geometric surface area of the 2-mm Pt disk electrode, of the Pt/PEDOT-PB modified electrode was 57.32 mA M^{-1} cm^{-2}. Due to this low sensitivity obtained for continuous monitoring of H_2O_2 concentration, electrochemical detection of H_2O_2 at this Pt/PEDOT-PB modified electrode was further investigated. To this end, the chronoamperograms were recorded at 0.0 V vs. Ag/AgCl for different H_2O_2 concentrations ranging from $1x10^{-5}$ M to $1x10^{-4}$ M in discontinuous operation mode, i.e. the analyte is injected into the electrochemical cell and the current is then recorded for a certain period of time during potentiostatic polarization of the electrode. Current is measured at the end of the polarization step, followed by a new increment in analyte concentration. This approach was used to obtain linear dependence of current vs. concentration (see Fig. 9B). The correlation coefficient (R^2) of 0.9955 and the sensitivity of 105.10 mA M^{-1} cm^{-2} yielded better performances for application in analysis of the PEDOT-PB coating with respect to H_2O_2 reduction under this operation mode. The lower limit of the linear calibration range considered as the detection limit is 10^{-5} M. The results obtained showed that the Pt/PEDOT-PB modified electrode is suitable for further analytical applications in electrochemical sensors. The analytical performances of other hydrogen peroxide sensors are presented in Table 3.

Figure 9 near here

Table 3 near here

Table 3 shows that the analytical performances of the PEDOT-PB-soluble modified electrode are comparable with those reported in the literature [43-47]. Furthermore, the pure PEDOT-ClO_4 and the PEDOT-FeCN coatings showed no response to hydrogen peroxide reduction under the same experimental conditions, a behavior that demonstrates the usefulness of PEDOT-PB composite materials in hydrogen peroxide detection.

4. Conclusions

The composite inorganic-organic coatings consisting of PEDOT-PB, and organic polymer doped with ferricyanide, PEDOT-FeCN, were prepared using electrochemical methods. In-situ preparation of the PB inside the organic matrix was achieved via cyclic voltammetry using various multiple potential cycles. Electrochemical behavior of the composite inorganic-organic coatings is based mainly on inorganic component redox reactions. A variation in roughness values from 3 nm to 217 nm for PEDOT-ClO_4 and PEDOT-FeCN, PEDOT-PB coatings, respectively, was observed. SEM and AFM measurements revealed a granular pattern of the deposited inorganic mediator inside the organic polymer matrix. This granular pattern is the result of a nucleation mechanism followed by aggregation of PB nanoparticles. Although the adhesion properties of the composite materials are clearly different, all the films lead to a decrease in adhesive force that can be useful for applications in micromanipulation. Promising results were obtained concerning electrochemical detection of hydrogen peroxide using chronoamperometry at these modified electrodes. The results obtained in this work thus clearly demonstrate the versatility of the preparation procedures by providing full control of film thickness and the analytical applications of the composite coating in sensor fabrication.

Acknowledgements

S. Lupu acknowledges extensively the Visiting Professor stage at the University of Franche-Comté, Besançon, France. Authors gratefully thank the platform MIMENTO of FEMTO-ST Institute in Besançon, France. This work was also supported by the EU under FAB2ASM (contract FoF-NMP-2010-260079): Efficient and Precise 3D Integration of Heterogeneous Microsystems from Fabrication to Assembly, and by the French National Agency (ANR) under NANOROL (contract ANR-07-ROBO-0003): Nanoanalyse for micromanipulate. The force measurement taken by Atomic Force Microscopy was taken on the "Nanorol platform" (The "Nanorol platform" can be used by external persons. Availability and booking of the station are consultable via internet on: http://nanorol.cnrs.fr/events.php.

REFERENCES

[1] S.G. Penn, L. Hey, M.J. Natan, Curr. Opin. Chem. Biol. 7 (2003) 609.

[2] L. Agui, P. Yanez-Sedeno, J.M. Pingarron, Anal. Chim. Acta 622 (2008) 11.

[3] R. Gupta, A. Kumar, Biotechnol. Adv. 26 (2008) 533.

[4] M. Haga, K. Kobayashi, K. Terada, Coord. Chem. Rev. 251 (2007) 2688.

[5] N. Rozlonik, Anal. Bioanal. Chem. 395 (2009) 637.

[6] D. Nicolas-Debarnot, F. Poncin-Epaillard, Anal. Chim. Acta 475 (2003) 1.

[7] B. Adhikari, S. Majumdar, Prog. Polym. Sci. 29 (2004) 699.

[8] B. Lakard, G. Herlem, M. de Labachelerie, W. Daniau, G. Martin, J.-C. Jeannot, L. Robert, B. Fahys, Biosens. Bioelectron. 19 (2004) 595.

[9] B. Lakard, O. Segut, S. Lakard, G. Herlem, T. Gharbi, Sens. Actuators, B 122 (2007) 101.

[10] A.A. Karyakin, Electroanalysis 13 (2001) 813.

[11] F. Ricci, G. Palleschi, Biosens. Bioelectron. 21 (2005) 389.

[12] S. Lupu, Rev. Roum. Chim. 50 (2005) 207.

[13] S. Lupu, Rev. Roum. Chim. 50 (2005) 213.

[14] Y. Liu, Z. Chu, W. Jin, Electrochem. Commun. 11 (2009) 484.

[15] F. Qu, A. Shi, M. Yang, J. Jiang, G. Shen, R. Yu, Anal. Chim. Acta 605 (2007) 28.

[16] A. Goux, J. Ghanbaja, A. Walcarius, J. Mater. Sci. 44 (2009) 6601.

[17] R. Koncki, O.S. Wolfbeis, Anal. Chem. 70 (1998) 2544.

[18] S. Lupu, Rev. Roum. Chim. 51 (2006) 525.

[19] S. Lupu, L. Pigani, R. Seeber, F. Terzi, C. Zanardi, Collect. Czech. Chem. Commun. 70 (2005) 154.

[20] K. Itaya, H. Akahashi, S. Toshima, J. Electrochem. Soc. 129 (1982) 1498.

[21] K. Itaya, N. Shoji, I. Uchida, J. Am. Chem. Soc. 106 (1984) 3423.

[22] L. He, C.-S. Toh, Anal. Chim. Acta 556 (2006) 1.

[23] P.J. Kulesza, K. Miecznikowski, M. Malik, M. Gałkowski, M. Chojak, K. Caban, A. Wieckowski, Electrochim. Acta 46 (2001) 4065.

[24] S.N. Sawant, N. Bagkar, H. Subramanian, J.V. Yakhim, Philos. Mag. 11 (2004) 2127.

[25] M. Ocypa, A. Michalska, K. Maksymiuk, Electrochim. Acta 51 (2006) 2298.

[26] A.I. Melato, L.M. Abrantes, A.M. Botelho do Rego, Thin Solid Films 518 (2010) 1947.

[27] A. Lisowska-Oleksiak, A.P. Nowak, Solid State Ionics 179 (2008) 72.

[28] M. Wilamowska, A. Lisowska-Oleksiak, J. Power Sources 194 (2009) 112.

[29] A.P. Nowak, M. Wilamowska, A. Lisowska-Oleksiak, J. Solid State Electrochem. 14 (2010) 263.

[30] A. Lisowska-Oleksiak, A.P. Nowak, M. Wilamowska, M. Sikora, W. Szczerba, Cz. Kapusta, Synth. Met. 160 (2010) 1234.

[31] V. Noël, H. Randriamahazaka, C. Chevrot, J. Electroanal. Chem. 489 (2000) 46.

[32] A. Lisowska-Oleksiak, A.P. Nowak, V. Jasulaitiene, Electrochem. Commun. 8 (2006) 107.

[33] A. Lisowska-Oleksiak, A.P. Nowak, J. Power Sources 173 (2007) 829.

[34] S. Lupu, C. Lete, M. Marin, N. Totir, P.C. Balaure, Electrochim. Acta 54 (2009) 1932.

[35] M. Dietrich, J. Heinze, G. Heywang, F. Jonas, J. Electroanal. Chem. 369 (1994) 87.

[36] C. Kvarnstrom, H. Neugebauer, S. Blomquist, H.J. Ahonen, J. Kankare, A. Ivaska, Electrochim. Acta 44 (1999) 2739.

[37] L. Adamczyk, P.J. Kulesza, K. Miecznikowski, B. Palys, M. Chojak, D. Krawczyk, J. Electrochem. Soc. 152 (2005) E98.

[38] F. Li, S. Dong, Electrochim. Acta 32 (1987) 1511.

[39] R. Koncki, Crit. Rev. Anal. Chem. 32 (2002) 79.

[40] O. Segut, B. Lakard, G. Herlem, J.Y. Rauch, J.C. Jeannot, L. Robert, B. Fahys, Anal. Chim. Acta 597 (2007) 313.

[41] S. Lupu, F.J. Del Campo, F.X. Munoz, J. Electroanal. Chem. 639 (2010) 147.

[42] S. Lupu, N. Totir, Collect. Czech. Chem. Commun. 75 (2010) 835.

[43] M.P. O'Halloran, M. Pravda, G.G. Guilbault, Talanta 55 (2001) 605.

[44] E.A. Puganova, A.A. Karyakin, Sens. Actuators, B 109 (2005) 167.

[45] Y. Liu, Z. Chu, W. Jin, Electrochem. Commun. 11 (2009) 484.

[46] K.-S. Tseng, L.-C. Chen, K.-C. Ho, Sens. Actuators, B 108 (2005) 738.

[47] A. Ernst, O. Makowski, B. Kowalewska, K. Miecznikowski, P.J. Kulesza, Bioelectrochemistry 71 (2007) 23.

Captions for figures

Fig. 1. Schematic drawing of platinum electrode chips.

Fig. 2. Cyclic voltammograms recorded during electrochemical polymerization of EDOT at the Pt electrode chip in an aqueous solution containing 0.01 M EDOT and 0.1 M $LiClO_4$ as a supporting electrolyte. Potential scan rate: 0.05 V s^{-1}. The first 5 (A) and the first 10 consecutive scans (B) are depicted, respectively.

Fig. 3. Cyclic voltammograms recorded during electrodeposition of PEDOT-FeCN film at the Pt electrode in an aqueous solution containing 0.01 M EDOT and 0.1 M $K_3Fe(CN)_6$. Potential scan rate: 0.05 V s^{-1}. The first 5 consecutive scans (A) and 10 consecutive scans (B) are depicted.

Fig. 4. Cyclic voltammograms recorded at the Pt/PEDOT-FeCN modified electrodes prepared by 5 potential cycles (A) and 10 potential cycles (B) in an aqueous solution containing 0.002 M $FeCl_3$, 0.1 M KCl and 0.01 M HCl. Potential scan rate: 0.05 V s^{-1}. The first 5 (A) and 10 (B) consecutive scans are depicted.

Fig. 5. Cyclic voltammograms recorded at the Pt/PEDOT-PB modified electrodes prepared by 5 potential cycles (A) and 10 potential cycles (B) in an aqueous solution containing 0.1 M KCl and 0.01 M HCl. Potential scan rate: 0.05 V s^{-1}. The first 5 scans are depicted. (C) The cyclic voltammograms recorded in 0.1 M KCl and 0.01 M HCl aqueous solution at the Pt/PEDOT-PB modified electrodes prepared by 5 and 10 potential cycles, respectively.

Fig. 6. AFM images of composite coatings: (a): Pt/PEDOT-FeCN-5 scans, (b): Pt/PEDOT-FeCN-10, (c): Pt/PEDOT-PB-5, (d): Pt/PEDOT-PB-10, (e): Pt/PEDOT-ClO_4-5, (f): Pt/PEDOT-ClO_4-10.

Fig. 7. SEM images of composite coatings: (a): Pt/PEDOT-FeCN-5 scans, (b): Pt/PEDOT-FeCN-10, (c): Pt/PEDOT-PB-5, (d): Pt/PEDOT-PB-10, (e): Pt/PEDOT-ClO_4-5, (f): Pt/PEDOT-ClO_4-10.

Fig. 8. Force-distance curves for different polymer films electrodeposited on Pt substrates. (a): influence of the number of cycles for PEDOT electrodeposited with ClO_4^-, (b): influence of salt for 5 scans.

Fig. 9. (A) Chronoamperogram recorded at Pt/PEDOT-PB modified electrode during H_2O_2 reduction in 0.1 M phosphate buffer solution. H_2O_2 increment: 10 µM. Working potential: 0.00 V. Insert: current versus H_2O_2 concentration plot. (B) Calibration plot for the Pt/PEDOT-PB modified electrode used in discontinuous operation mode.

Table 1: Roughness of composite films. H: sample height, Ra: average roughness, Rq: peak to peak roughness.

Table 2: Pull-in force and Pull-off force of composite films.

Table 3. Comparison of the analytical performances of various PB based hydrogen peroxide sensors.

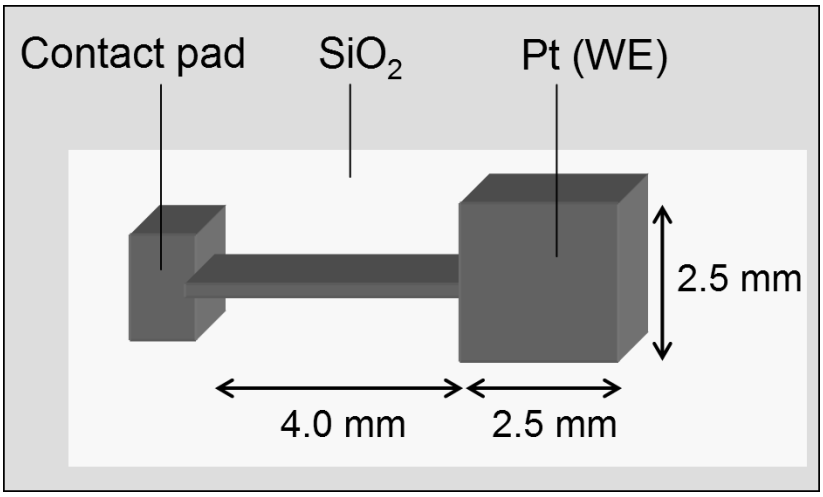

Fig. 1.

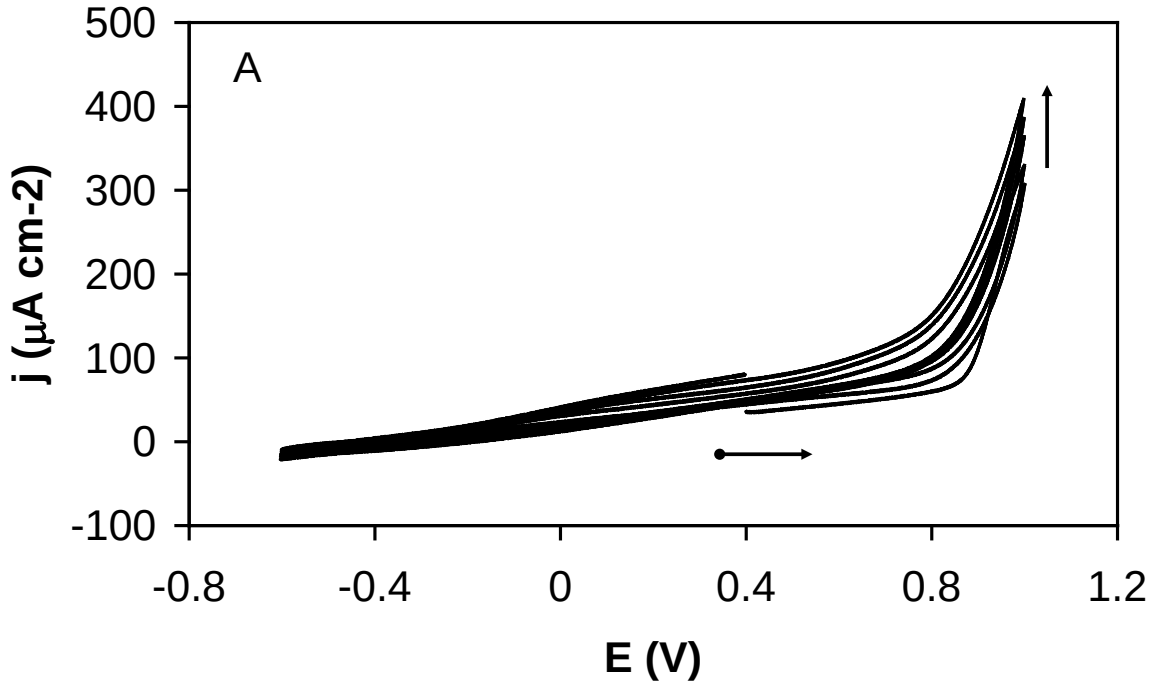

Fig. 2A.

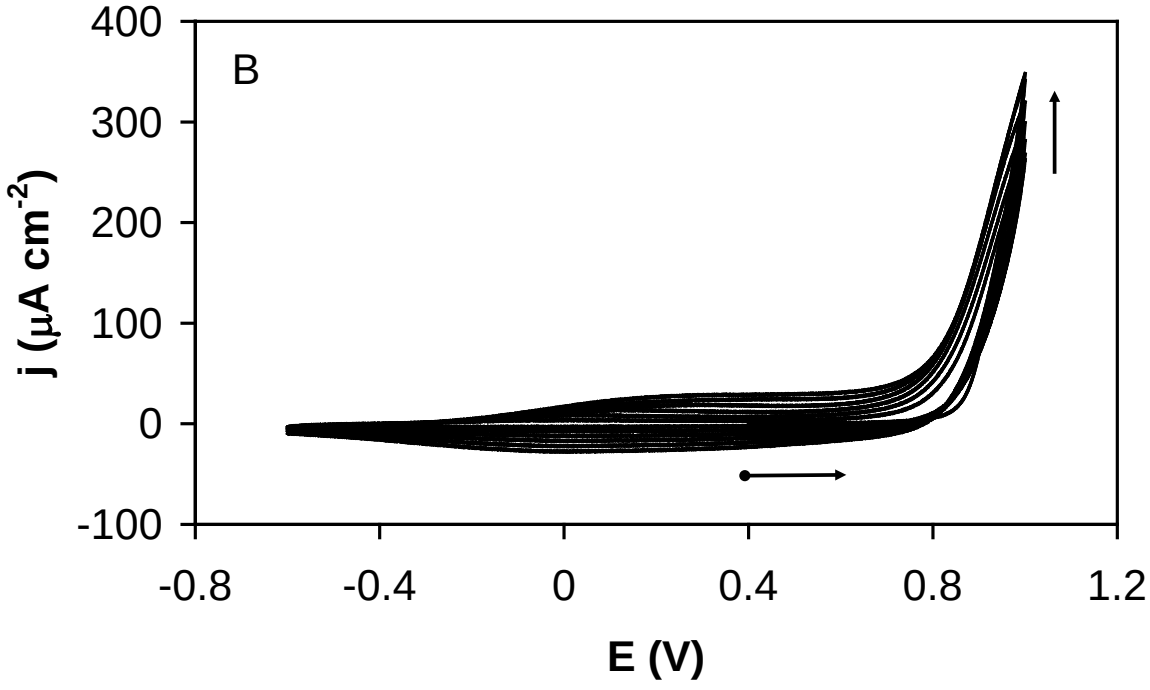

Fig. 2B.

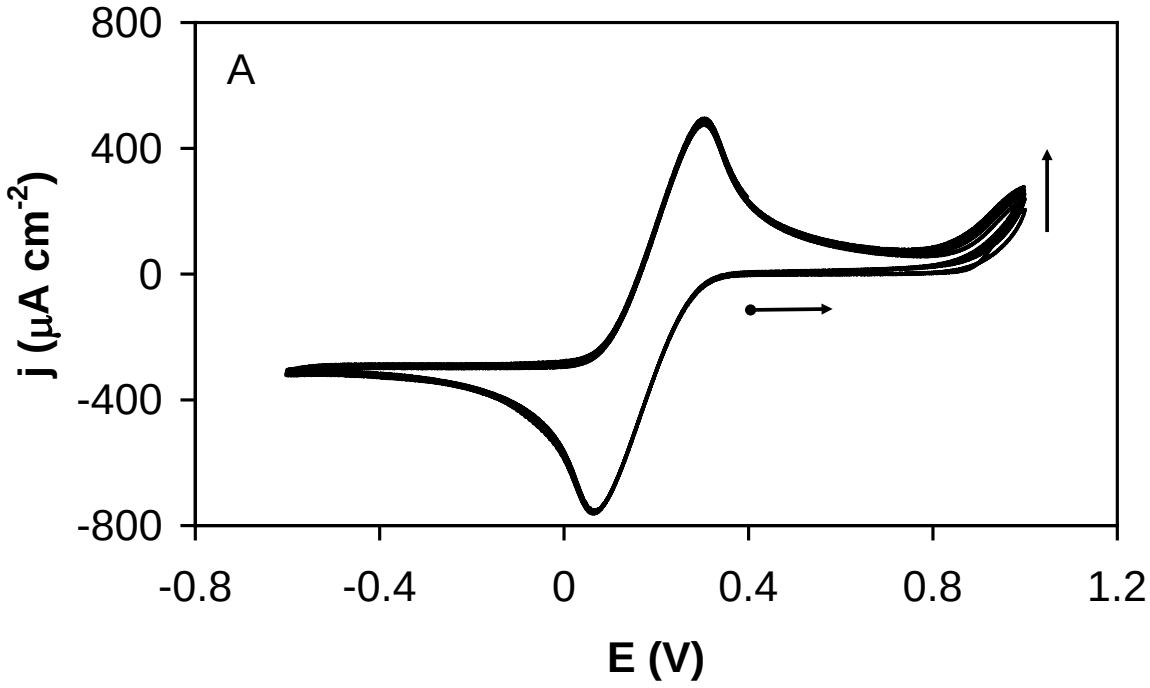

Fig. 3A.

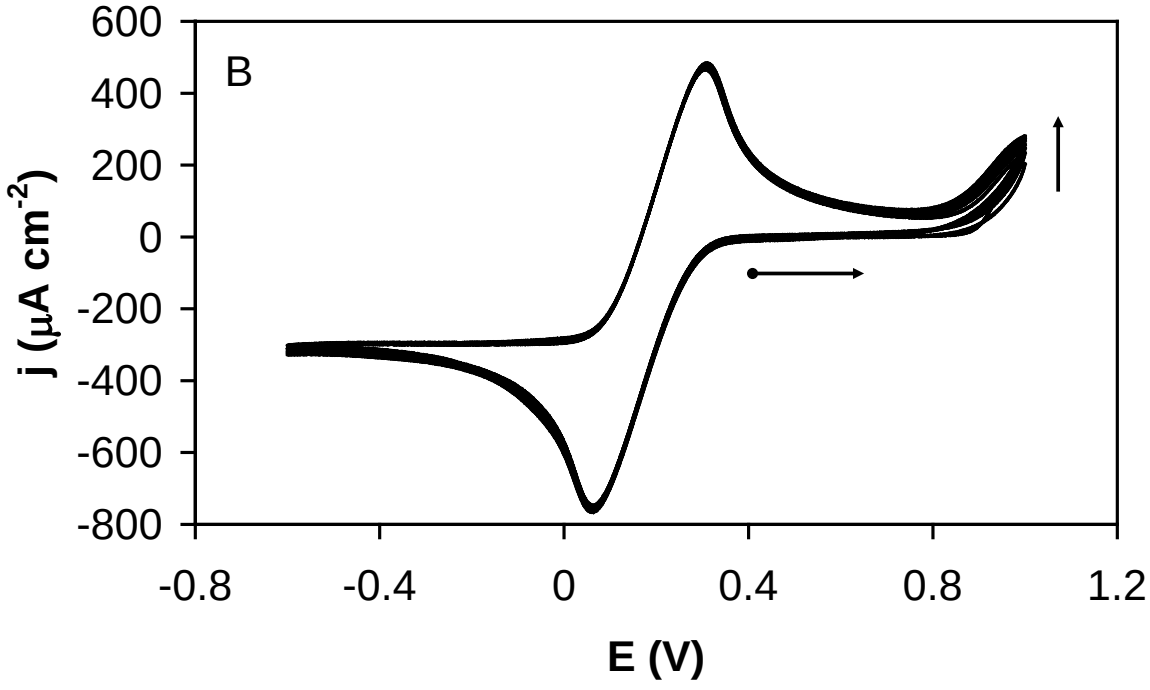

Fig. 3B.

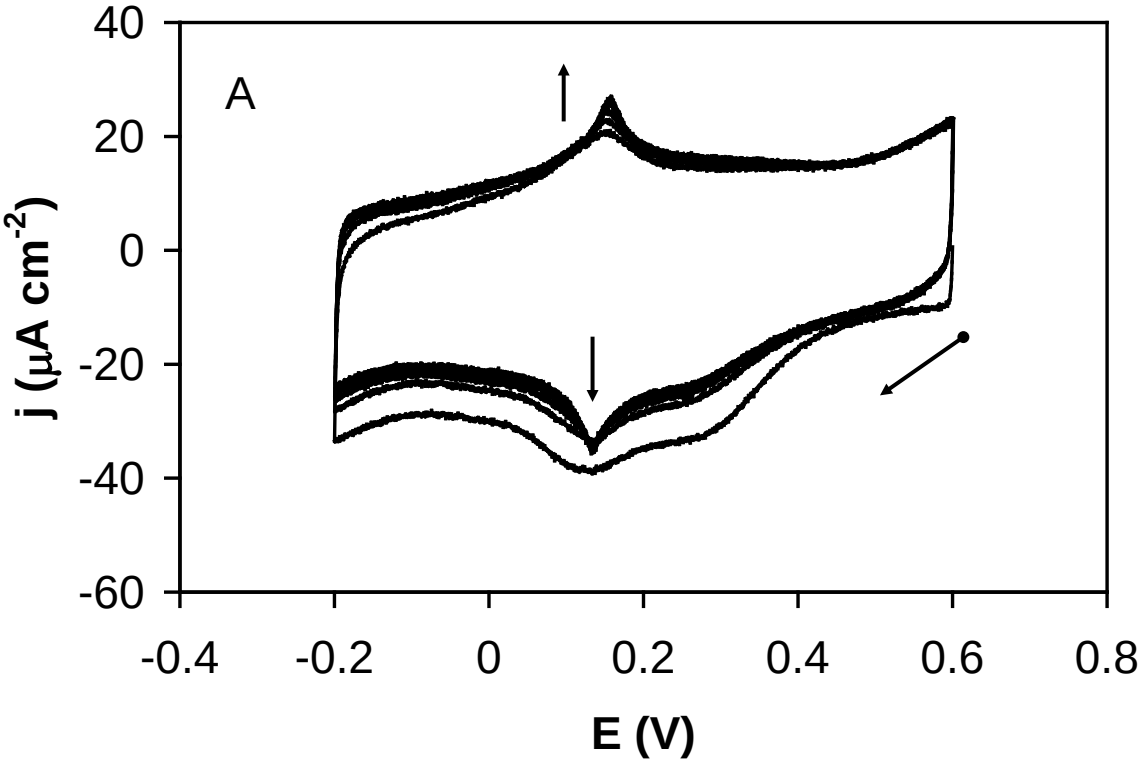

Fig. 4A.

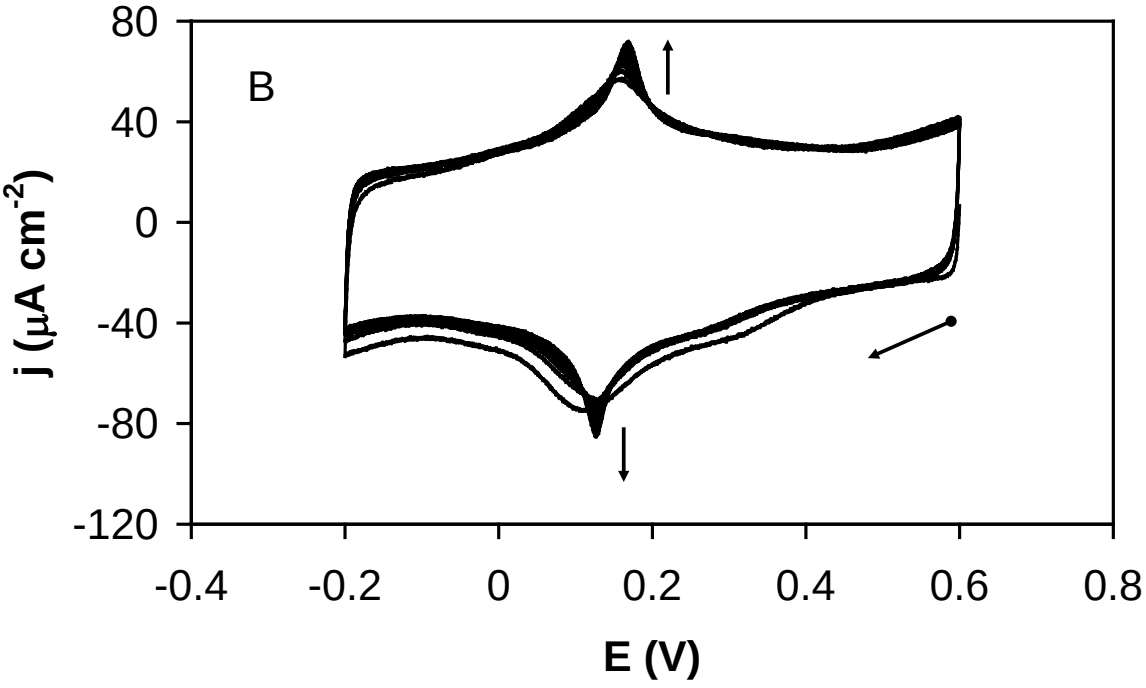

Fig. 4B.

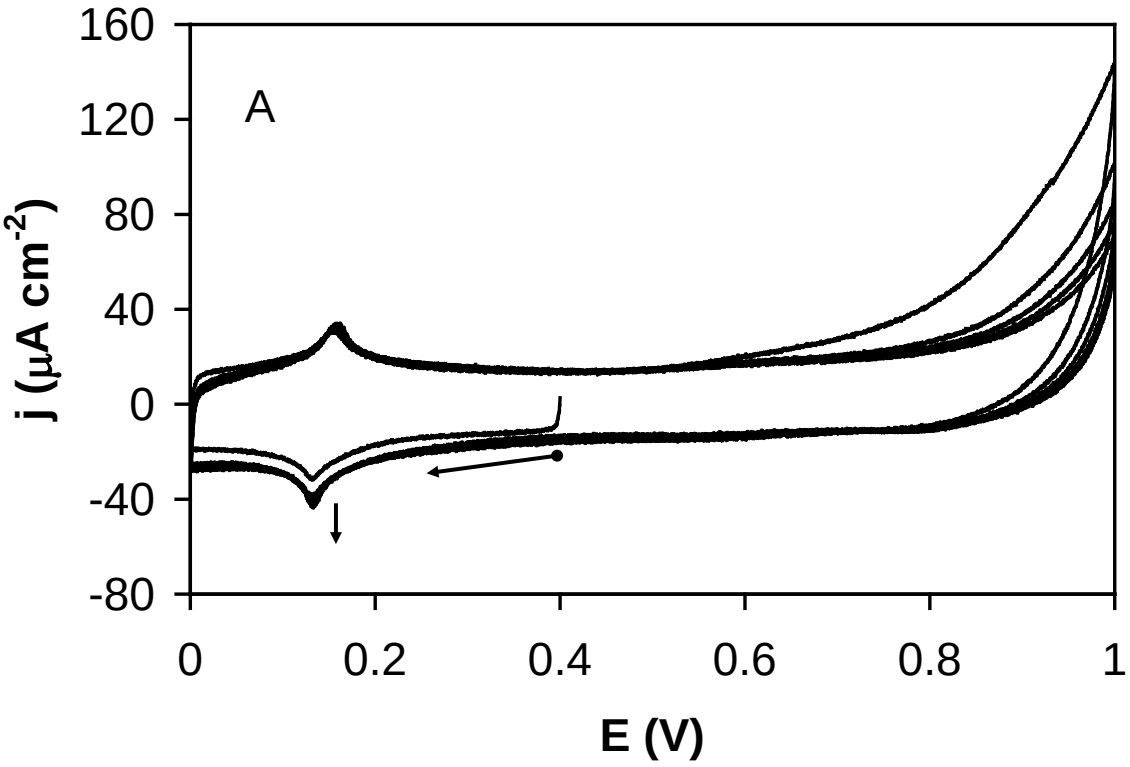

Fig.5A.

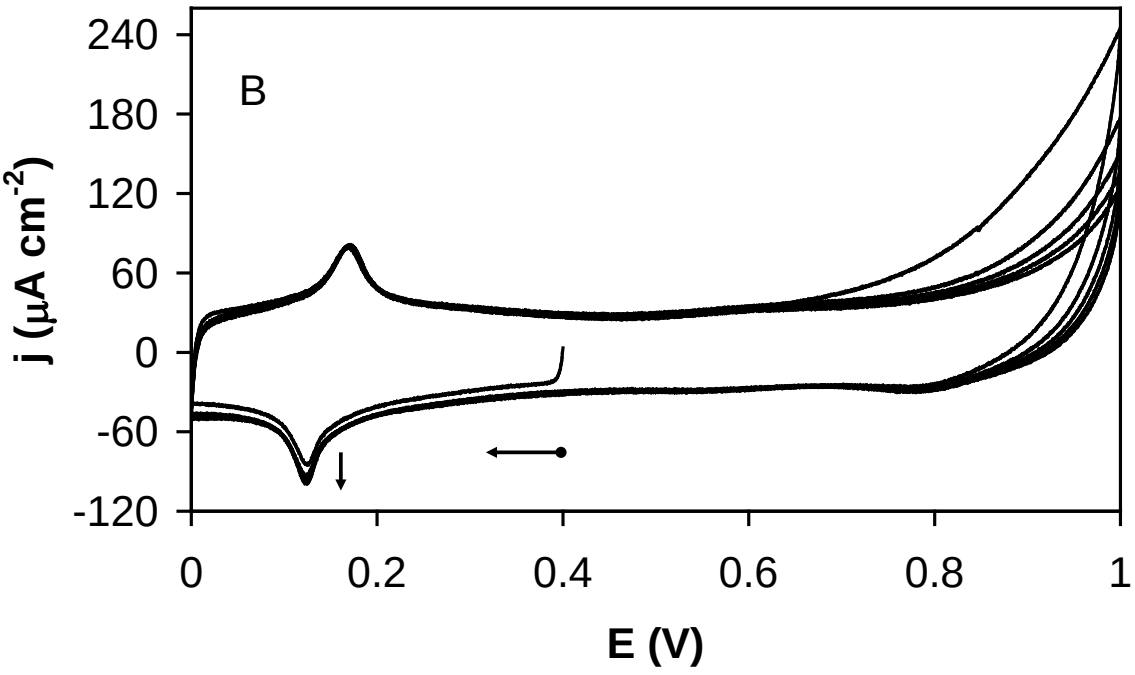

Fig. 5B.

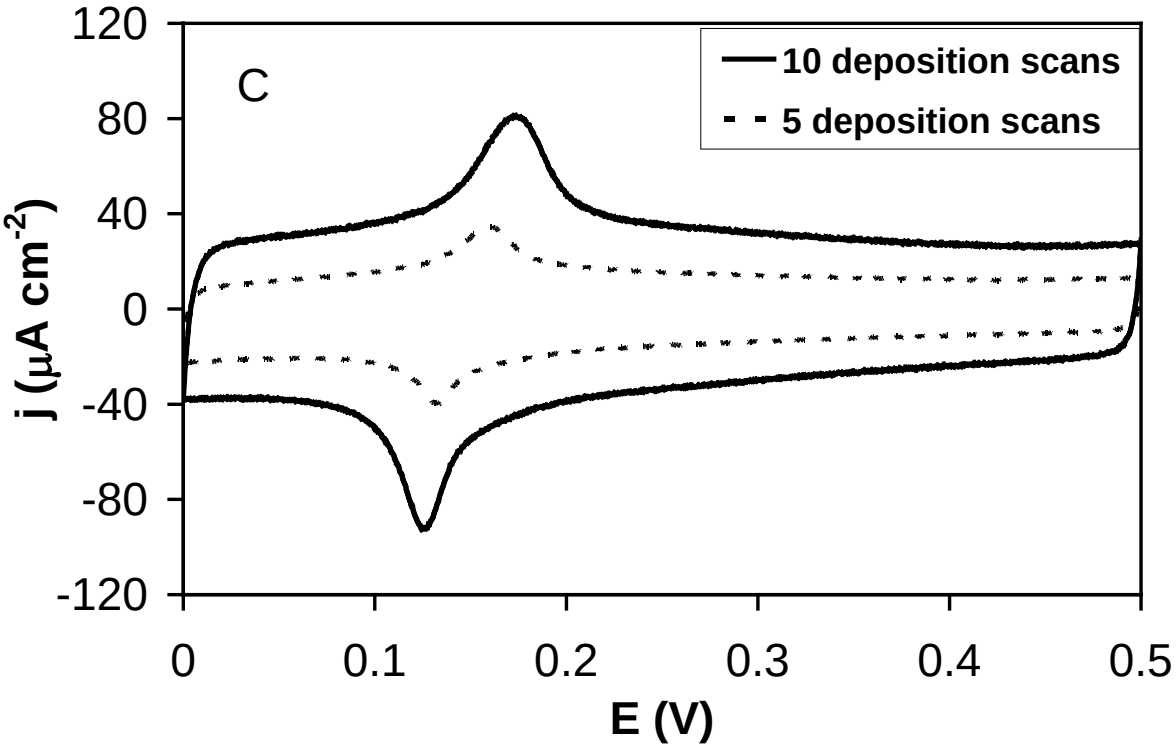

Fig. 5C.

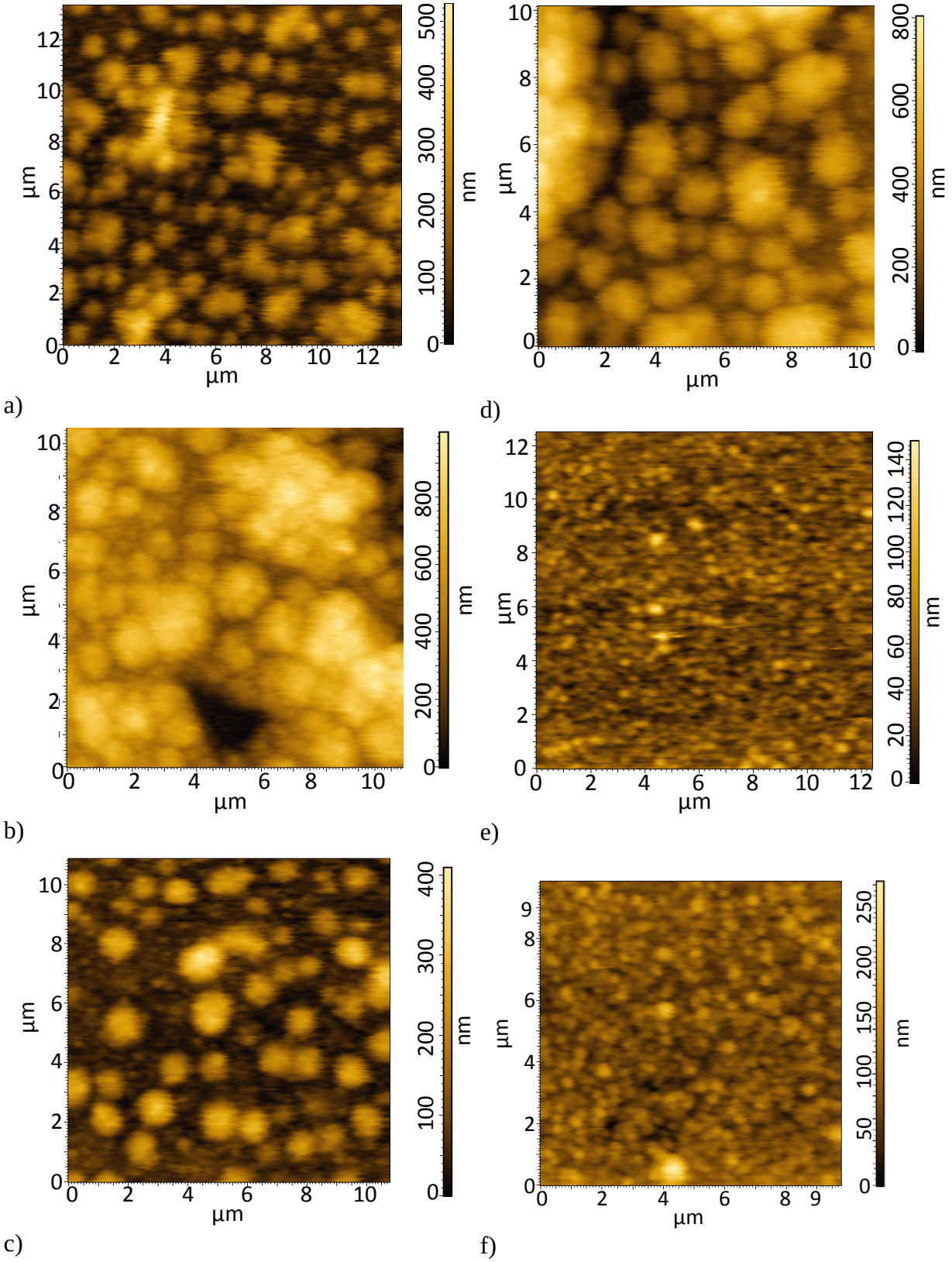

Fig. 6.

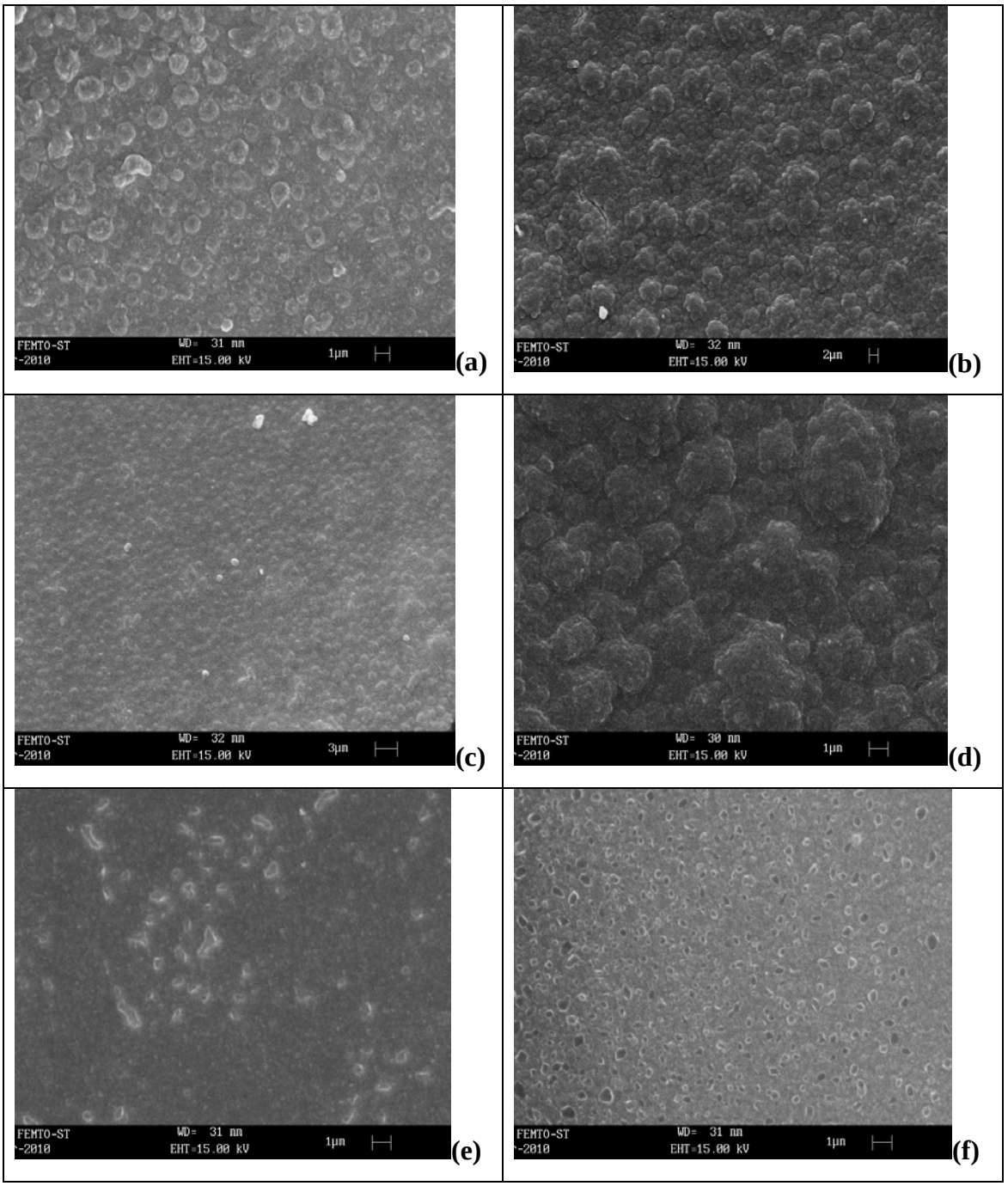

Fig. 7.

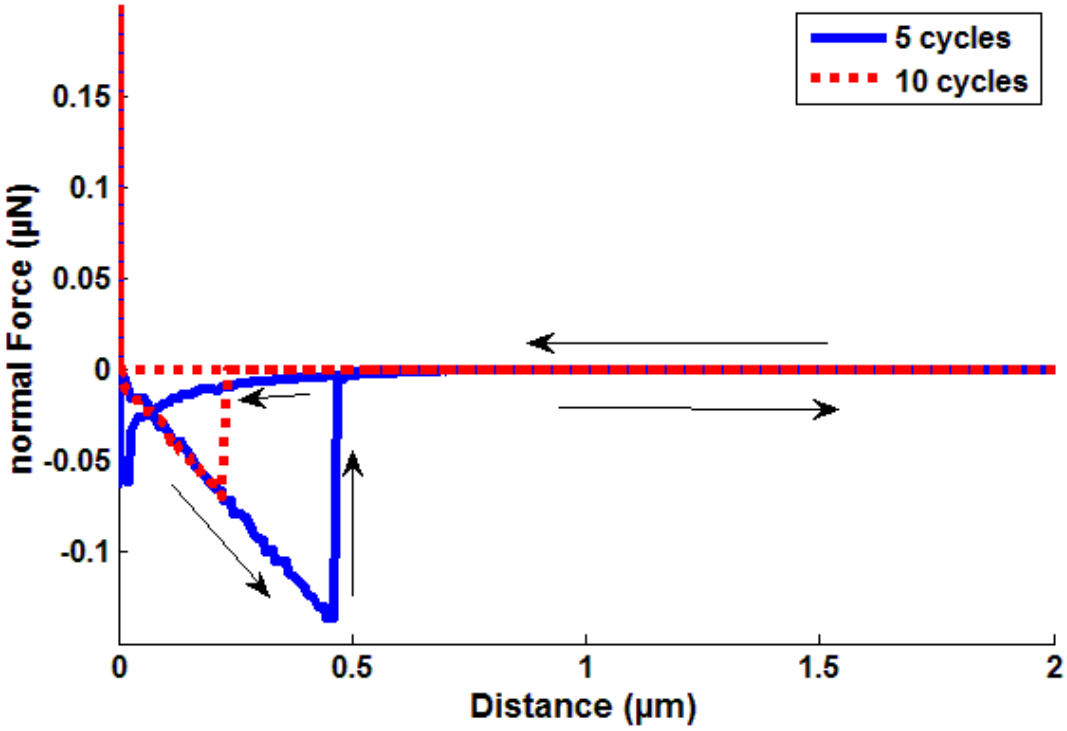

a)

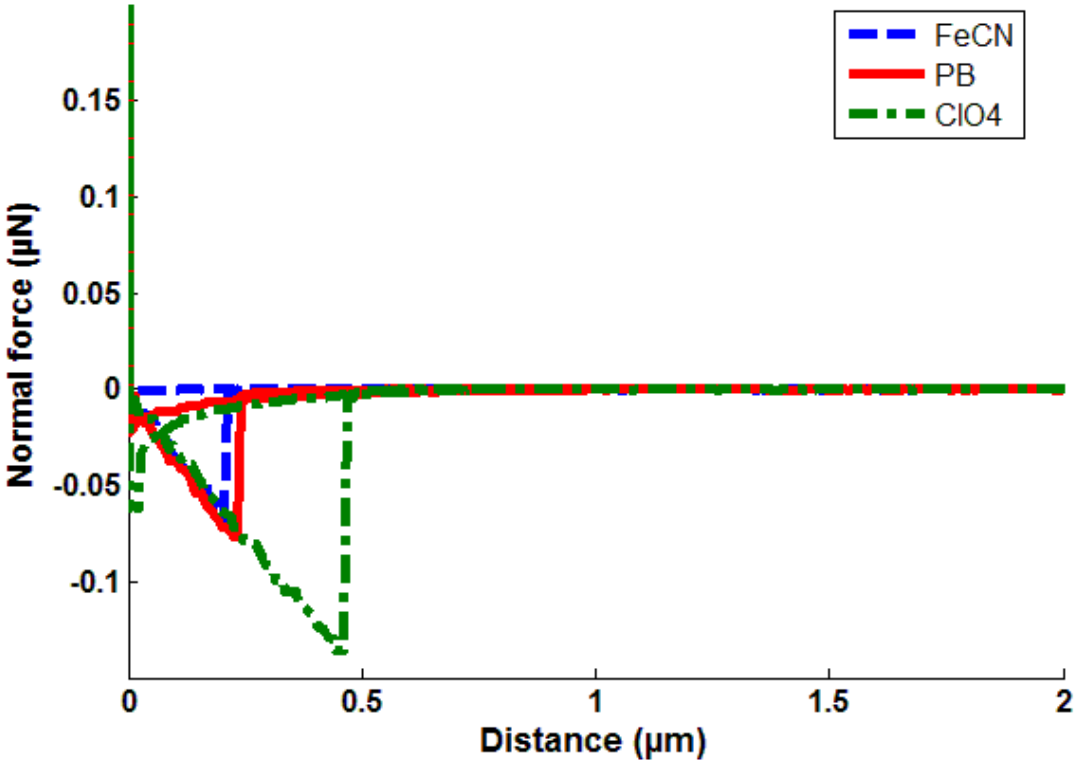

b)

Fig. 8.

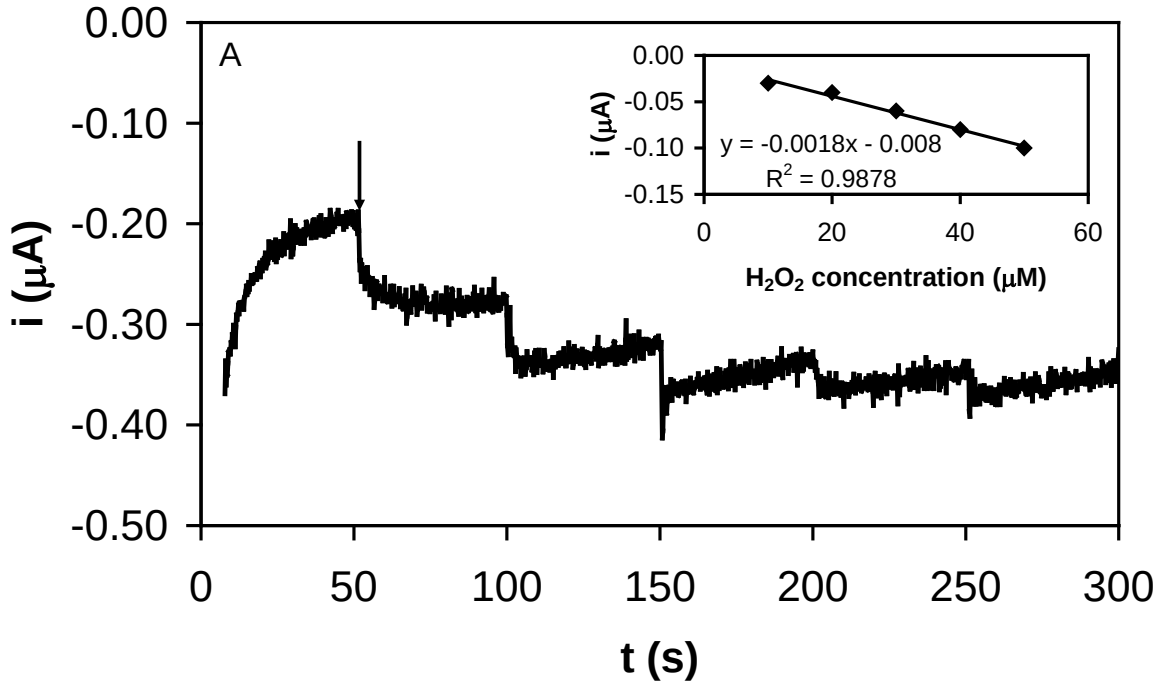

Fig. 9A.

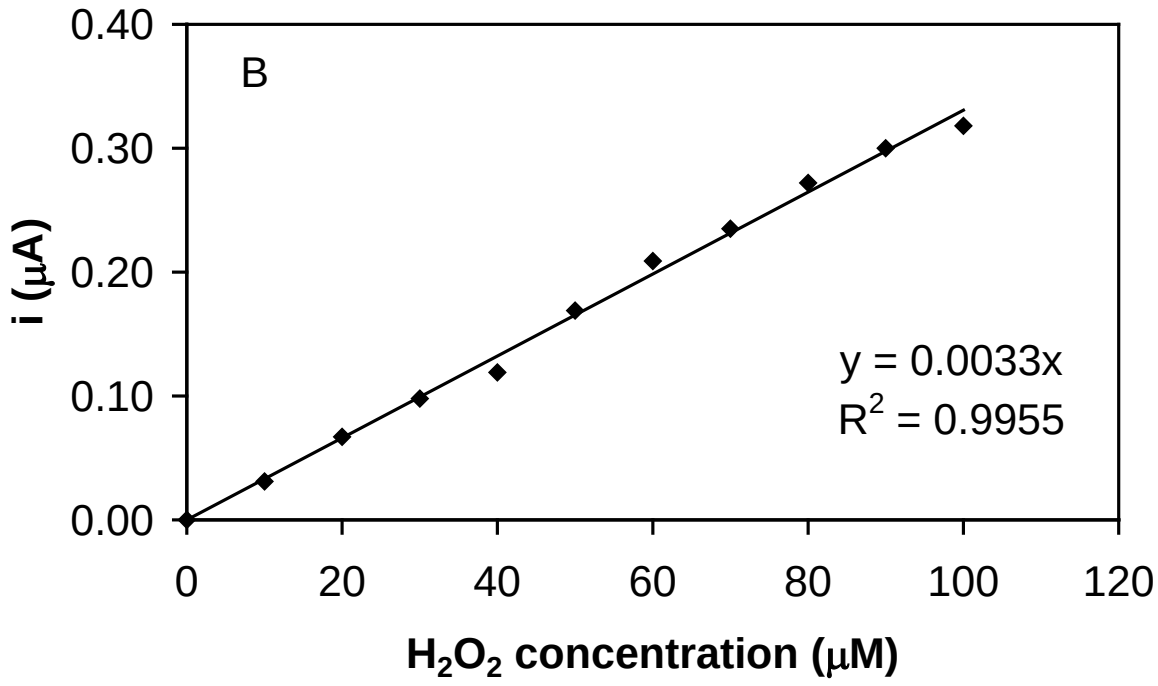

Fig. 9B.

Sample	Profilometry measurements		AFM measurements
Pt/PEDOT-FeCN-5	H = 1.094 µm	R_a = 24.55 nm R_q = 36.28 nm	R_a = 62.30 nm R_q = 77.97 nm
Pt/PEDOT-FeCN-10	H = 2.802 µm	R_a = 136.70 nm R_q = 174.11 nm	R_a = 171.63 nm R_q = 216.60 nm
Pt/PEDOT-PB-5	H = 0.775 µm	R_a = 13.87 nm R_q = 19.33 nm	R_a = 50.25 nm R_q = 64.03 nm
Pt/PEDOT-PB-10	H = 1.475µm	R_a = 95.67 nm R_q = 120.96 nm	R_a = 138.96 nm R_q = 172.16 nm
Pt/PEDOT-ClO_4-5	H = 0.566 µm	R_a = 4.32 nm R_q = 5.54 nm	R_a = 12.08 nm R_q = 15.64 nm
Pt/PEDOT-ClO_4-10	H = 1.181 µm	R_a = 3.09 nm R_q = 4.37 nm	R_a = 18.32 nm R_q = 23.99 nm

Table 1

Sample	Pull-in force	Pull-off force
Free polymer substrate	- 1 nN	< - 400 nN
Pt/PEDOT-FeCN-5	-2 nN	-66.3 nN
Pt/PEDOT-FeCN-10	-3 nN	-94.6 nN
Pt/PEDOT-PB-5	-30 nN	-82.7 nN
Pt/PEDOT-PB-10	-5 nN	-60.9 nN
Pt/PEDOT-ClO_4-5	-62 nN	-139.0 nN
Pt/PEDOT-ClO_4-10	-2 nN	-66.7 nN

Table 2

E l e c t r o d e	**Linear range (M)**	**Sensitivity (mA M^{-1} cm^{-2})**	**Potential applied (V)**	**Reference**
PB/SPE[a]	$4x10^{-7}$ to $1x10^{-4}$	137	0.00 V vs. Ag/AgCl	43
Nanostructured-PB/GC[b]	1×10^{-8} to 1×10^{-2}	200	0.00/0.05 V vs. Ag/AgCl	44
Self-assembled PB/Pt[c]	$1x10^{-6}$ to $4x10^{-4}$	625	-0.05 V vs. Ag/AgCl	45
PB/FTO[d]	$5x10^{-5}$ to $5x10^{-2}$	58.1	-0.20 V vs. Ag/AgCl	46
HRP-PEDOT/PB-PpyBA/GC[e]	N/A	N/A	0.20 V vs. Ag/AgCl	47
PEDOT-PB/Pt	$1x10^{-5}$ to $1x10^{-4}$	105.1	0.00 V vs. Ag/AgCl	This work

Table 3

[a]SPE: screen-printed electrode, [b]GC: glassy carbon, [c]Pt: platinum, [d]FTO: fluorine-doped tin oxide, [e]HRP: horseradish peroxidase, and PpyBA: poly(4(pyrrole-1-yl)-benzoic acid).